A Dislocation-Based Model for Variant Selection during the γ-to-α' Transformation

N.J. WITTRIDGE, J.J. JONAS, and J.H. ROOT

A phase transformation model is described for variant selection during the austenite-to-martensite transformation. The model depends entirely on the presence of glide dislocations in the deformed austenite. The direct correlation between the 24 slip systems of the Bishop and Hill (B–H) crystal plasticity model and the 24 ⟨112⟩ rotation axes of the Kurdjumov–Sachs (K–S) orientation relationship is employed. Two selection criteria, based on slip activity and permissible dislocation reactions, govern the variants that are chosen to represent the final transformation texture. The development of the model *via* analysis of the experimental results of Liu and Bunge is described. The model is applied to the four distinct strain paths: (1) plane strain rolling, (2) axisymmetric extension, (3) axisymmetric compression, and (4) simple shear. Experimental deformation and transformation textures were produced for comparison purposes *via* appropriate deformation and quenching procedures. In each case, the transformation texture predicted using the dislocation reaction model is in excellent agreement with the experimental findings.

I. INTRODUCTION

THE dislocation reaction model for variant selection during the austenite-to-martensite transformation was first proposed in detail by Sum and Jonas.[1] Unlike previous models,[2–5] which involved grain shape and residual stress considerations, the dislocation reaction model is based entirely on the presence of dislocations in the deformed austenite. It relies upon the one-to-one correspondence between the 24 possible Bishop and Hill (B–H) slip systems[6,7] and the 24 Kurdjumov–Sachs (K–S) transformation products[8]. The two simple variant selection criteria that form the basis of the model can be described as (1) the positive slip criterion and (2) the dislocation reaction criterion. The former specifies that only "positive slip" dislocations (defined in more detail subsequently) play a role in the transformation, while the latter allows for the in-plane reaction of glide dislocations.

The present model was derived *via* examination of the experimental results of Liu and Bunge, who studied the martensitic transformation in a Fe-30 pct Ni alloy containing a strong cube texture.[9] The initial single-component austenitic texture facilitated the assessment of the transformed martensitic components on an individual basis. Such a detailed examination of the transformation components allowed for the formulation of the two selection criteria used in the dislocation reaction model.

Subsequent efforts have concentrated on evaluating the validity of the dislocation reaction model for the four distinct strain paths: (1) plane strain rolling,[10,11,12] (2) axisymmetric extension,[13] (3) axisymmetric compression,[14] and (4) simple shear.[15] Using a similar methodology for each strain path, the model was applied to an appropriate simulated deformation texture with the aim of predicting the transformation texture. Textures calculated according to the two selection criteria were examined separately before they were combined to produce the final predictions. These were then compared with the corresponding experimental textures. For each strain path investigated, excellent agreement was found between the predicted transformation textures and the experimental findings.

The results of three of these investigations have only been presented in conference proceedings,[10–14] and so are not widely available. Furthermore, only a preliminary, approximate attempt was made to model the transformation of the compressed specimen,[14] so these calculations are repeated here in more detail. It is the objective of this article to present the new results and to provide a comprehensive summary of the previous investigations. This is combined with a description of the dislocation reaction model.

The present publication is divided into six sections. The first provides a complete description of the model, while the second outlines the Liu and Bunge[9] results and the derivation of the selection criteria. The next three sections describe the predictions of the model for deformation by plane strain rolling, axisymmetric extension/compression, and simple shear, respectively. The final section is concerned with a possible physical interpretation of the role of the slip dislocations.

II. THE DISLOCATION REACTION MODEL

The present approach is based on the observation[2] that there is a one-to-one correspondence between the 24 fcc slip systems that can be defined using the B–H notation[6,7] and the 24 possible bcc variants produced according to the K–S orientation relationship.[8] The B–H approach was devised independently of K–S; according to this notation, the four fcc slip planes and the three Burgers vectors per plane can be labeled as shown in Figure 1. As there are two possible slip directions per Burgers vector, there is a total of 24 possible slip systems. The first 12 slip systems (including slip plane and slip direction) are represented in Table I using

Dr. N.J. WITTRIDGE is Materials Selection Engineer with Granta Design Ltd., Trompington, Cambridge, U.K. J.J. JONAS, Professor, is with the Department of Metallurgical Engineering, McGill University, Montreal, PQ, Canada H3A 2B2. J.H. ROOT, Program Leader, is with the Steacie Institute for Molecular Sciences, Chalk River Laboratories, Chalk River, ON, Canada K0J 1J0.

Manuscript submitted December 6, 1999.

REPRODUCED BY PERMISSION OF THE MINISTER OF SUPPLY AND SERVICES CANADA

the B–H convention. The second 12 systems merely involve the negatives of the Burgers vectors of the systems given in Table I.

The K–S transformation can be characterized as involving +90 deg rotations about each of the 24 ⟨112⟩ rotation axes that relate the parent and product crystals. The indices of a particular ⟨112⟩ axis are obtained from the cross-product of the plane normal and the Burgers vector that make up the fcc slip system. These rotations are equivalent to the following K–S parallelism conditions:

$$\{111\}_\gamma \,//\, \{110\}_\alpha$$

$$\langle -101\rangle_\gamma \,//\, \langle 1{-}11\rangle_\alpha$$

Four alternatives exist for the plane parallelism and 6 for the direction condition, resulting in the 24 possible variants. Figure 1 indicates that the K–S rotation axes are perpendicular to the respective slip directions or Burgers vectors lying on the "a" slip plane.

For each parent orientation of interest, the shear rates on the 24 possible slip systems are calculated using a suitable computer program. In the present case, a rate-sensitive crystal plasticity model was used with a value of $m = 0.05$. However, a rate-insensitive model can be employed just as well. Depending on the symmetry of the orientation, a different number of slip systems will be activated. The original parent orientations are then used to calculate the 24 corresponding product orientations using the appropriate ⟨112⟩ rotation axes of the K–S transformation. At this stage, the first selection criterion is applied and only those systems characterized by positive or active shear are selected. Positive slip is defined as slip in the direction of the resolved (applied) shear stress. By this means, the "negative" slip systems are eliminated, that is, those with Burgers vectors opposite in sign to the positive slip vectors. (Similar remarks apply to the rotation axes, where a negative rotation axis corresponds to a rotation of −90 deg about a "positive" axis.) Such negative slip Burgers vectors had been used in earlier analyses.[2] This approach is shown here to be in error.

The shortcomings of previous slip activity models indicate that additional variants, not selected by the slip activity criterion, are necessary to complete the predictions. The second selection criterion of the present model utilizes the concept of in-plane reactions between glide dislocations to account for the presence of these missing variants. Reactions take place when dislocations of two different Burgers vectors located on a common slip plane (or on parallel slip planes aided by cross-slip) combine to produce a new product vector originally rejected by the positive shear criterion. In this case, two *active* dislocations react to produce a single *inactive* product dislocation. This is shown schematically in Figure 2. The reactions occur according to certain well-known rules.[16] For example, for active slip systems ±aI and ±aII (using the B–H notation), only the following in-plane reactions are possible:

$$\text{aI} + \text{aII} = -\text{aIII}$$

$$(-\text{aI}) + (-\text{aII}) = \text{aIII}$$

Given that there are 24 slip systems for a particular crystal, there is a possible $24 \times 24 = 576$ reactions. However, due to reasons of symmetry, most of these are redundant, leaving a total of 216 distinct cases. These are shown in Table II, where six different types of interactions can be identified: (1) cross-slip, (2) annihilation, (3) Lomer–Cottrell lock formation, (4) energy increase (no reaction possible), (5) in-plane reaction, and (6) reactions requiring cross-slip. As explained in detail elsewhere,[10,11,12] it is only the in-plane reactions that are relevant to the present discussion, while all the other types of interaction can be eliminated.

The lower left-hand half of Table II represents the 72 "positive-positive" cases corresponding to the interactions

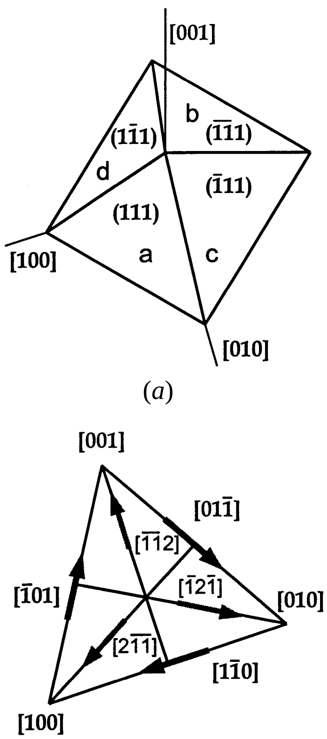

Fig. 1—(*a*) One half of the octahedron formed by the four {111} planes employed in the present version of the Bishop and Hill notation.[6,7] (*b*) The ⟨110⟩ and ⟨112⟩ directions associated with plane a.

Table I. Slip Systems, as Defined by Bishop and Hill and Their Associated ⟨112⟩ Axes[6,7]

Plane or Axis	Slip System and Corresponding ⟨112⟩ Rotation Axis											
	a (111)			b ($\bar{1}\bar{1}$1)			c ($\bar{1}$11)			d (1$\bar{1}$1)		
{111}	I	II	III	I	II	III	I	II	III	I	II	III
⟨110⟩	[01$\bar{1}$]	[$\bar{1}$01]	[1$\bar{1}$0]	[0$\bar{1}\bar{1}$]	[101]	[$\bar{1}$10]	[01$\bar{1}$]	[101]	[$\bar{1}\bar{1}$0]	[0$\bar{1}\bar{1}$]	[$\bar{1}$01]	[110]
⟨112⟩	[2$\bar{1}\bar{1}$]	[$\bar{1}$2$\bar{1}$]	[$\bar{1}\bar{1}$2]	[$\bar{2}$1$\bar{1}$]	[1$\bar{2}\bar{1}$]	[112]	[211]	[$\bar{1}\bar{2}$1]	[$\bar{1}$1$\bar{2}$]	[$\bar{2}\bar{1}$1]	[121]	[1$\bar{1}\bar{2}$]

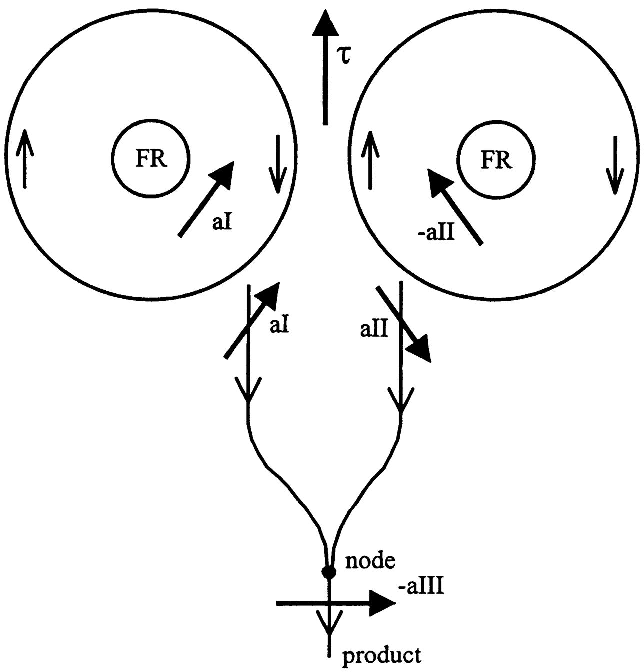

Fig. 2—Schematic diagram of a typical in-plane dislocation reaction illustrating the dislocation loops emanating from two Frank–Read (FR) sources and the enforced parallelism of the dislocation line vectors that reverses one of the Burgers vectors deduced from the slip activity program.

of pairs of positive dislocations. There is an equivalent set of 72 “negative-negative” interactions (not shown here) that can be deduced directly from the lower half of the table by changing the signs of the reactants and products. The upper right-hand half represents the “positive-negative” interactions; it also describes the “negative-positive” interactions, as the combination of (aI) + (−cI), for example, leads to the same result as (−cI) + (aI).

The newly selected vectors, labeled “reaction” products, contribute to the final transformation texture *via* the appropriate rotation axis listed in Table I (or its opposite). The rules for dislocation reactions are given in Weertman and Weertman;[16] their use for the present purpose is described in more detail in Jonas and Wittridge.[10] In what follows, the orientations that cannot be formed as a result of dislocation reaction are labeled “no reaction” variants, while the remaining ones that are not selected are referred to as “miscellaneous.”

It should be added that the geometry of dislocation reactions obliges the line vectors of the reacting dislocations to be parallel when the Burgers vectors are summed. As the line vectors of adjacent Frank–Read type loops are opposed by definition (Figure 2), the sign of one of the Burgers vectors selected by the slip activity program must be reversed. This is how the “forbidden” combination of aI + (−aII) in Figure 2, which would lead to an energy *increase*, is converted into the allowable one of aI + aII. In the present work, the sign of the *more active* slip system (aI in the previous example) is conserved, while that of the less active in-plane system is reversed. When the two reacting systems are equally active, both the negative and positive products can be formed.

Finally, the positive slip variants and the permissible reaction variants are combined in particular ratios to produce the predicted transformation texture. Each variant is given a weight first according to the intensity of its parent orientation and second according to the amount of shear with which it is associated. In the case of the reaction components, the weights are assigned according to the lesser shear value of the two slip systems involved in the reaction.

III. FORMULATION OF THE DISLOCATION REACTION MODEL

As mentioned previously, the dislocation reaction model was deduced by analysis of the experimental results of Liu and Bunge.[9] The Fe-30 pct Ni alloy used in their experiments was selected for the stability of the austenitic phase at room temperature. This permitted determination of the texture of the austenite phase prior to transformation, something that cannot readily be done in the case of steel. The alloy transforms to martensite below −100 °C and this phase is retained when the material returns to room temperature, allowing the texture to be measured once more.

Specimens possessing a strong cube texture were cold rolled to 10 pct reduction along different angles with respect to the initial rolling direction of [010]. The five parent orientations, generated by rolling at 0, 11, 21, 31, and 45 deg to the rolling direction, were the following: (001)[0-10], (001)[−1-50], (001)[−2-50], (001)[−3-50], and (001)[−1-10], respectively (Figure 3). The small rolling reduction applied to the originally cube-oriented specimens resulted in samples possessing a single component (plus a random background) prior to transformation, each of which was part of the cube fiber. By means of rolling, sufficient strain had been applied to introduce the dislocations that led to variant selection. Following rolling, transformation to martensite was induced *via* quenching in liquid nitrogen (−196 °C).

For the sake of brevity, only the results pertaining to a single direction, namely, 11 deg from the rolling direction, will be presented in this article. The transformation texture in the form of the (200) pole figure reported by Liu and Bunge for this sample is shown in Figure 4(a). This texture was simulated by Sum and Jonas[1] using the dislocation reaction model by employing the following approach.

(1) All possible variants calculated according to the K–S transformation law were identified and tabulated together with their associated B–H slip systems and K–S rotation axes (Table III).
(2) The shear rates for plane strain rolling applicable to each slip system were calculated for a single increment of von Mises applied strain using a rate-sensitive slip analysis and added to the table mentioned previously.
(3) The two selection criteria that were described in the previous section were then applied. This allowed identification of the two sets of predicted texture components.
(4) A pole figure was plotted indicating the simulated transformation texture.

The upper row of Table III lists all the possible product orientations (in the form of Miller indices) that can be formed from the parent orientation according to K–S. The first three columns of the table (from the left) represent the 24 B–H slip systems and their associated K–S rotation axes. The

Table II. Grid of Possible In-Plane and Other Reaction Products

Reactants	−aI	−aII	−aIII	−bI	−bII	−bIII	−cI	−cII	−cIII	−dI	−dII	−dIII
aI		x 112	x 121	x 020	x 112	xx aII −dIII	ANN	x 112	x 121	x 020	x 112	LC −bII −cII
aII	−aIII		x 211	x 112	x 200	xx −aI −cI	x 112	x 200	LC −bI −dI	x 112	ANN	x 211
aIII	−aII	−aI		xx bII cII	xx bI dI	C/S	x 121	LC dI bI	x 200	LC bII cII	x 211	x 020
bI	x 200	LC cIII −dIII	x 121		x 112	x 112	x 020	x 112	LC −aII −dII	ANN	x 112	x 121
bII	LC dIII -cIII	x 002	x 211	−bIII		x 112	x 112	ANN	x 211	x 112	x 200	LC −aI −cI
bIII	x 121	x 211	ANN	−bII	−bI		LC aII dII	x 211	x 020	x 121	LC aI cI	x 200
cI	C/S	xx −aIII bIII	xx −dII −aII	x 200	xx dIII −cIII	x 121		x 112	x 112	x 020	x 112	xx −bII −cII
cII	xx −cIII dIII	x 002	x 211	xx aIII −bIII	C/S	xx −bI −dI	−cIII		x 112	x 112	x 200	xx −aI −cI
cIII	xx −cII −dII	x 211	x 020	x 121	xx −aI −cI	x 200	−cII	−cI		xx aII dII	xx bI dI	C/S
dI	x 002	xx cIII −dIII	x 121	C/S	xx aIII −bIII	xx −bII −cII	x 002	LC aIII −bIII	x 112		x 112	x 112
dII	xx bIII −aIII	C/S	xx −cI −aI	xx cIII −dIII	x 200	x 211	LC −aIII bIII	x 002	x 112	−dIII		x 112
dIII	x 121	xx −bI −dI	x 200	xx −aII −dII	x 211	x 200	x 112	x 112	ANN	−dII	−dI	
Reactants	aI	aII	aIII	bI	bII	bIII	cI	cII	cIII	dI	dII	dIII

Notes: (1) The in-plane reaction products are shown lightly shaded.
(2) The reaction products that could form as a result of intersection are heavily shaded.
(3) The reactions that would lead to an energy increase are indicated with an "x."
(4) Lomer-Cottrell locks are labeled "LC."

products are labeled "observed" and "not observed" in accordance with the experimental findings. The filled symbols represent the products that were selected, while the open symbols refer to the products that were eliminated using the present model. The predicted pole figure that corresponds to this table is illustrated in Figure 4(b). For comparison, the measured texture has been reproduced on this diagram in the form of contour lines.

For the (001)[−1-50] parent orientation, employment of the positive shear criterion leads to the selection of (100)[023] as the associated transformation component. This orientation is represented by the star symbol in Figure 4(b). It can be attributed to the following active slip systems and shear rates: aI (0.82), bI (0.82), cI (0.36), dI (0.36), −aII (0.033), −bII (0.033), −cII (0.015), and −dII (0.015). Of interest to note in Figure 4(a) is the presence of four "subspots" near the center of the pole figure. These spots are associated with the relatively heavy slip experienced by systems aI, bI, cI, and dI. In contrast, the lighter slip experienced by systems −aII, −bII, −cII and −dII does not lead to subspots that can be distinguished from the background intensity in this area. (It should be remarked in passing that the presence of the four subspots in Figure 4(a), and of similar subspots in their other pole figures, led Liu and Bunge to conclude that the transformation took place by the N–W mechanism, rather than by that of K–S. It is shown here that the four subspots can be attributed instead to the operation of four highly active slip systems, while still retaining the validity of the K–S mechanism.) The (110)[−115] and (110)[001] orientations, which are associated with the negatives of the aforementioned eight slip systems, are eliminated and are not actually observed experimentally. They are represented by the open square and open trapezoid symbols of Figure 4(b).

The additional symbols visible on the pole figure correspond to variants associated with unstressed dislocations;

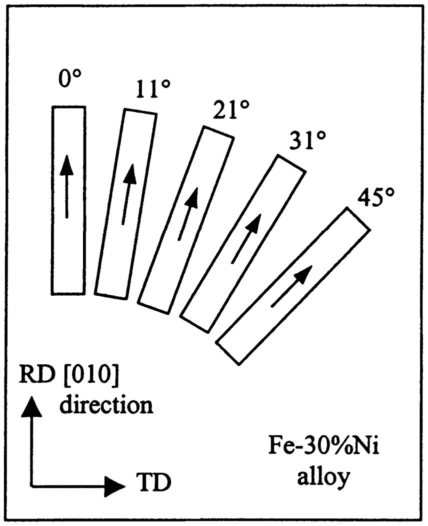

Fig. 3—Schematic diagram indicating the five directions of deformation with respect to the original [010] rolling direction.

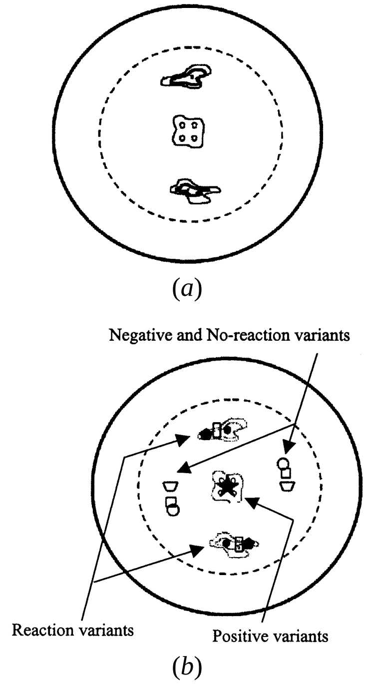

Fig. 4—(*a*) Reproduction of the (200) pole figure from Liu and Bunge's experimental transformation texture for the (001)[−1-50] parent orientation.[9] (*b*) (200) pole figure of the predicted transformation texture (full symbols) for the (001)[−1-50] parent orientation.[9] Open symbols represent K–S variants that are not selected by the present approach.

here they are denoted as "R" (reaction product) or "NR" (no reaction is able to take place) on Table III. For the current parent, orientations (110)[−110] (filled circle) and (110)[−221] (filled pentagon) result from the reaction products −cIII, −dIII and −aIII, −bIII, respectively, and are denoted by R on Table III. Similarly, (110)[−114] (open circle) and (110)[001] (open trapezoid) correspond to slip systems cIII, dIII and aIII, bIII, respectively, and are labeled NR as no reaction can take place to produce them. As mentioned previously, these orientations are not observed in the

Table III. Active Slip Systems, Shear Rates, Permissible Reactions, and Predicted Transformation Texture Components for the (001) [−1-50] Parent Orientation.[1]

			Observed				Not Observed		
Variant	Slip System	Rotation Axis	(100)[023] ★	(110)[−110] ●	(110)[−331] □	(110)[−221] ⬟	(110)[−114] ○	(110)[−115] □	(110)(001) ⏢
1	−bIII	−1 −1 −2	—	—	—	R	—	—	—
2	−dIII	−1 1 2	—	R	—	—	—	—	—
3	−cIII	1 −1 2	—	R	—	—	—	—	—
4	−aIII	1 1 −2	—	—	—	R	—	—	—
5	dII	1 2 1	—	—	−0.015	—	—	—	—
6	bII	1 −2 −1	—	—	−0.033	—	—	—	—
7	aII	−1 2 −1	—	—	−0.033	—	—	—	—
8	cII	−1 −2 1	—	—	−0.015	—	—	—	—
9	−cI	−2 −1 −1	—	—	—	—	—	−0.36	
10	−aI	−2 1 1	—	—	—	—	—	—	−0.82
11	−bI	2 −1 1	—	—	—	—	—	—	−0.82
12	−dI	2 1 −1	—	—	—	—	—	−0.36	—
13	bIII	1 1 2	—	—	—	—	—	—	R N
14	dIII	1 −1 −2	—	—	—	—	R N	—	—
15	cIII	−1 1 −2	—	—	—	—	R N	—	—
16	aIII	−1 −1 2	—	—	—	—	—	—	R N
17	−dII	−1 −2 −1	0.015	—	—	—	—	—	—
18	−bII	−1 2 1	0.033	—	—	—	—	—	—
19	−aII	1 −2 1	0.033	—	—	—	—	—	—
20	−cII	1 2 −1	0.015	—	—	—	—	—	—
21	cI	2 1 1	0.36	—	—	—	—	—	—
22	aI	2 −1 −1	0.82	—	—	—	—	—	—
23	bI	−2 1 −1	0.82	—	—	—	—	—	—
24	dI	−2 −1 1	0.36	—	—	—	—	—	—

Table IV. Euler Angles, Active Slip Systems, Shear Rates, Permissible Reactions, and Cross-Slip Relationships for the Seven Selected Parent Orientations

Ideal Orientation	Euler Angles φ_1	Φ	φ_2	Positive Slip Systems and Shear Rates	Products before Cross-Slip	Products after Cross-Slip
Cu	90.0	35.3	45.0	c_{III} (1.4), $-d_{III}$ (1.4), a_I (0.4), $-a_{II}$ (0.4)	$\pm a_{III}$	$\pm b_{III}$
Cu-S	74.0	36.0	54.0	c_{III} (1.2), $-d_{III}$ (1.6), a_I (0.4), $-a_{II}$ (0.4)	$\pm a_{III}$	$\pm b_{III}$
S	58.9	36.7	63.4	c_{III} (0.9), $-d_{III}$ (1.7), a_I (0.5), $-a_{II}$ (0.4)	$-a_{III}$	$+b_{III}$
S-brass	46.1	34.5	76.0	c_{III} (0.7), $-d_{III}$ (1.6), a_I (1.1), $-a_{II}$ (0.2)	$-a_{III}$	$+b_{III}$
brass	35.3	45.0	90.0	$-d_{III}$ (1.2), a_I (1.2), $-c_I$ (0.4), c_{III} (0.4)	$\pm c_{II}$	$\pm b_{II}$
Brass-Goss	15.8	45.0	90.0	$-d_{III}$ (1.0), a_I (1.0), $-c_I$ (0.1), c_{III} (0.1), $-a_{III}$ (0.2), d_I (0.2)	d_{II}, $-a_{II}$, $\pm c_{II}$	d_{II}, $-a_{II}$, $\pm b_{II}$
Goss	0.0	45.0	90.0	$-d_{III}$ (0.6), a_I (0.6), $-a_{III}$ (0.6), d_I (0.6)	$\pm a_{II}$, $\pm d_{II}$	$\pm a_{II}$, $\pm d_{II}$

measured texture. The remaining transformation product, (110)[−331], was listed as an observed component by Liu and Bunge. Although its variants are associated with negative shear rates, the orientation is situated midway between two predicted components, (110)[−110] and (110)[−221]. Thus, its appearance can be justified in terms of the "overlap" of the Gaussian distribution of grain orientations about (110)[−110] and (110)[−221].

The same methodology was applied to the four remaining parent orientations, and in each case, the simulated transformation texture faithfully reproduced the experimental texture. The analysis thus provides verification of the suitability of the dislocation reaction model for predicting variant selection during the γ-to-α' transformation.

IV. PLANE STRAIN ROLLING

A. *Experimental Approach*

The dislocation reaction model has now been evaluated under conditions of plane strain rolling for a multicomponent starting texture. A detailed description of this investigation can be found in the conference proceedings listed as References 10 through 12. The fcc textures produced by plane strain rolling can be described by two continuous fibers. For simplicity, the two fibers were represented in the preceding study by seven discrete components: the copper {112}⟨111⟩, S {213}⟨364⟩, brass {110}⟨112⟩, and Goss {110}⟨001⟩, as well as the three intermediate orientations, Cu-S, S-brass, and brass-Goss.

Using an approach similar to that of Sum and Jonas,[1] all 24 product variants were identified for each of the seven parents using a rotation program that incorporates the 90 deg ⟨112⟩ K–S orientation relationship. The rate-sensitive slip activity program (m = 0.05) was then employed to apply an increment of plane strain deformation to each of the seven parent grains in turn. The results obtained in this way are listed in Table IV using the B–H notation to identify the appropriate slip systems. The table indicates only the positive slip variants. Note that a *positive* slip of, say, +1.6 on system −dIII indicates that a *negative* slip of −1.6 must exist on system dIII. As stated earlier, the *negative* slip variants are not used in the selection of variants.

All possible in-plane dislocation reactions were then evaluated for the active slip variants according to the dislocation reaction criterion described in Section II. This operation led to the reaction products listed in the fourth column of Table IV. However, for the case of fcc rolling, as well as for one of the other examples considered subsequently, a further rule was adopted regarding the reaction components. This was found to be necessary if the experimental rolling results were to be correctly reproduced. (This will be demonstrated in more detail later.) The rule states that a given reaction product will cross-slip onto a new plane as long as the latter is unstressed, *i.e.*, inactive. Thus, ±aIII in Table IV are converted into ±bIII, while ±cII become ±bII. (Note that none of the positive slip Burgers vectors in Table IV lie on the b plane, qualifying it as an inactive plane.) Although the reason why this cross-slip event should occur is not known at present, one possible explanation is provided subsequently. Unfortunately, the use of transmission electron microscopy to determine the exact Burgers vectors involved in the γ-to-α' transformation is somewhat impeded by the experimental difficulties associated with the presence of a ferromagnetic phase. The reaction products that are obtained after allowing for cross-slip are listed in the final column of Table IV.

B. *Prediction of the Transformation Texture*

The transformation texture obtained by summing the positive slip systems for all seven parents is illustrated in the φ_2 = 45 deg cross section of the orientation distribution function (ODF) space shown in Figure 5(a). Here, the strong influence of the brass orientation in the deformed austenite can be seen. Also notable is the absence of what is known as the transformed copper component, in the vicinity of $\varphi_1 = 0$ deg, $\Phi = 35$ deg. Plotting of the reaction components results in the texture indicated in the ODF section of Figure 5(b). The presence of the previously absent copper component is readily evident, which demonstrates that the latter arises directly from the reaction of in-plane glide dislocations. However, the appearance of the "transformed copper" orientation in the correct location (φ_1 = 0 deg, Φ = 35 deg) requires adoption of the "cross-slip rule" described in Section A. Note that Figures 5(a) and (b) were constructed without the use of any weights for the components.

For obvious reasons, not much is known about the specific intensities in the austenite rolling fiber. The dislocation reaction model prescribes that each variant is first weighted according to the amount of shear with which it is associated and second according to the intensity of the parent orientation. Here, the parent intensities were taken to be similar to those of rolled brass[11,12] (Table V).

The rolled brass intensities were employed in association with the corresponding shear rates to calculate the overall texture illustrated in Figure 5(c). Here, the positive slip

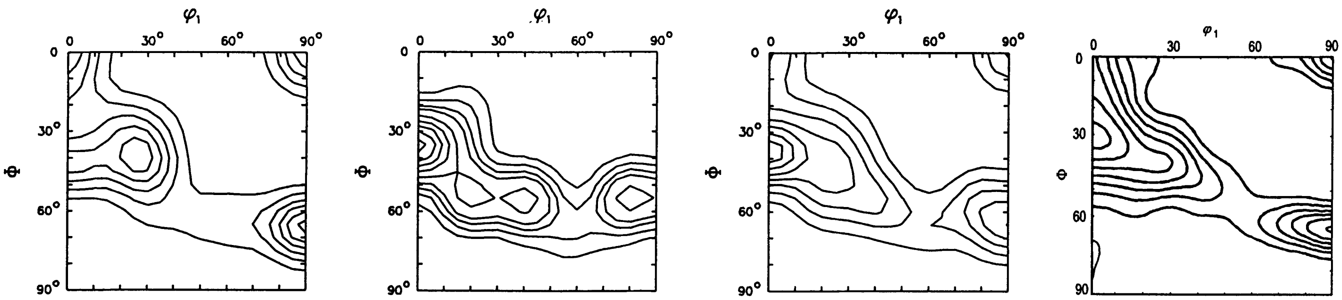

(a) (b) (c) (d)

Fig. 5—Superposition of the seven sets of (*a*) positive slip variants and (*b*) reaction product variants. (*c*) Present simulation of the transformation texture obtained by combining the positive slip and reaction product variants in the strength ratio 1:1.5. (*d*) Typical experimental transformation texture determined on a pancaked Nb steel.

Table V. Relative Intensities of the Seven Parents Representing the Fcc Rolling Fiber

Parent	Cu	Cu-S	S	S-Brass	Brass	Brass-Goss	Goss
Weight	0.4	0.4	0.5	0.6	1	0.8	0.4

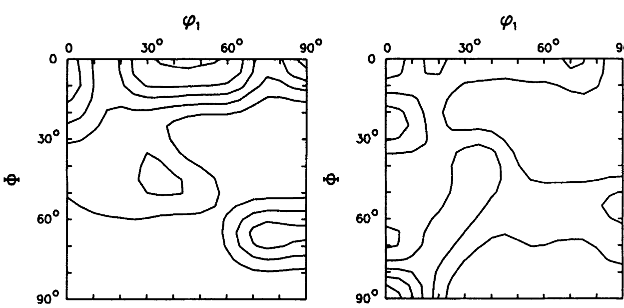

(a) (b)

Fig. 6—Superposition of the seven sets of (*a*) negative slip variants and (*b*) the remaining miscellaneous variants.

variants and reaction products of Figures 5(a) and (b) were combined with the appropriate final weights. In addition, the reaction products were given 1.5 times the influence or importance of the positive variants, because the reaction product variants always seem to be more intense than those attributable to positive slip (as demonstrated by the results of Liu and Bunge and the results for the other strain paths[1,9,13,15]). For reference, a typical experimental transformation texture determined on a pancaked Nb steel with a bainitic microstructure is shown in Figure 5(d). From a comparison of Figures 5(c) and 5(d), it is evident that the predicted texture is in excellent agreement with the experimental findings. It is also readily apparent that both the positive slip and the reaction product variants are necessary to achieve this result.

The importance of variant selection is further illustrated in Figure 6(a), which represents all the variants that have been excluded on the basis of negative slip. Here, the presence of the cube fiber and that of an intense {116}⟨110⟩ component are evident. These are not generally observed. Similarly, the components associated with the remaining rotation axes (*i.e.*, the miscellaneous variants) are displayed in Figure 6(b). If included, they would lead to the presence of the rotated Goss, {110} ⟨110⟩, and the cube fiber, which once again are not observed.

V. AXISYMMETRIC COMPRESSION AND EXTENSION

A. *Experimental Approach*

Application of the dislocation reaction model to transformation after deformation by axisymmetric compression or by axisymmetric extension was relatively straightforward due to the fact that in each case the deformation and transformation textures can be represented by fibers. More detailed descriptions of the two experiments are given in References 13 and 14. The first step for each investigation was to produce experimental deformation and transformation textures that could be used for comparison purposes.

An alloy similar to that used by Liu and Bunge, namely, Fe-30 pct Ni, was selected for the experiments. To produce the extension textures, a circular bar of diameter 12 mm was machined with the axial direction aligned parallel to the rolling direction of the original plate. The bar was subjected to a swaging/extension process at a starting temperature of 300 °C until a final diameter of 9.5 mm (*i.e.*, a reduction of 37 pct) was reached. For the compression textures, the axial direction was again aligned with the rolling direction and the samples were compressed to a reduction in height of 33 pct at a similar temperature. This temperature was chosen to avoid the formation of deformation-induced martensite.[17] Transformation was subsequently induced by quenching in liquid nitrogen at −196 °C. Neutron diffraction texture measurements were performed on the samples in both the deformed and transformed conditions using the E3 neutron diffractometer at the Chalk River Laboratories of Atomic Energy of Canada Limited (AECL). In each case, inverse pole figures were calculated from three complete pole figures for each of the austenite and martensite phases.

B. *Experimental Textures*

The deformation texture components of the compressed sample appear along the {110} fiber in the ODF (not shown) and can be seen as centered about ⟨110⟩ in the inverse pole figure of Figure 7(a). The transformed components are spread predominantly along the {111} fiber in the ODF (not shown) and are centered about ⟨111⟩ in Figure 8(a). Weaker components are also evident near ⟨110⟩ and along the ⟨*1vw*⟩

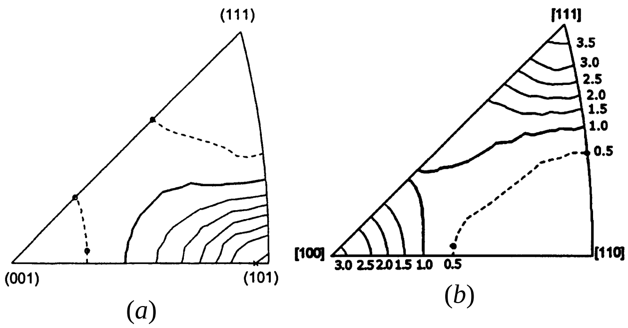

Fig. 7—Measured deformation textures for the (*a*) compression and (*b*) extension samples. Here, and in Figs. 8 through 12, contours intervals = 0.5, beginning with 0.5× random.

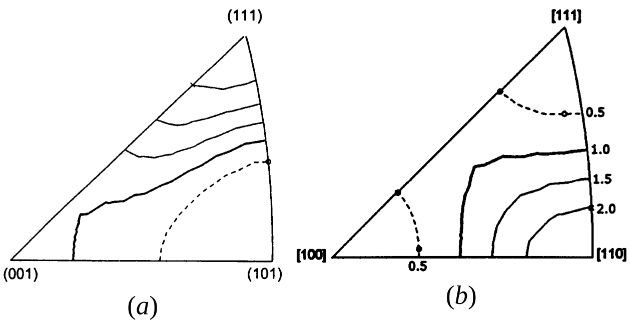

Fig. 8—Measured transformation textures for the (*a*) compression and (*b*) extension samples.

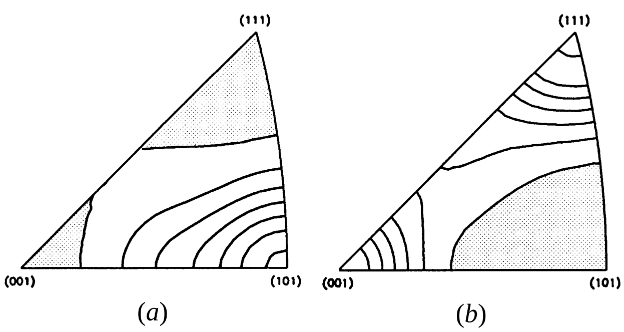

Fig. 9—Deformation texture simulated using the two sets of parent orientations selected for the (*a*) compression and (*b*) extension experiments.

fiber. The textures that characterize the extension samples are the reverse of the compression textures, as expected. The deformation texture is dominated by the ⟨111⟩ and ⟨100⟩ fibers, while minor components are visible along the ⟨*1vw*⟩ fiber (Figure 7(b)). After quenching, these components have transformed into orientations centered around ⟨110⟩ (Figure 8(b)).

C. *Prediction of the Transformation Texture*

For the accurate prediction of transformation textures, it is important to select the correct parent orientations to represent the deformation texture. The compression texture was simulated *via* 16 orientations along the ⟨110⟩ and ⟨210⟩ fibers (Figure 9(a), Table VI). Here, seven more parents are employed than in the earlier investigation.[14] For the extension texture, six orientations were chosen along the

Table VI. Parent Orientations Used in the Compression and Extension Simulations

Compression Fibers		Extension Fibers	
⟨110⟩ fiber	(1-10)[001]	⟨111⟩ fiber	(111)[1-10]
	(1-10)[113]	—	(111)[2-31]
	(1-10)[112]	—	(111)[1-21]
	(1-10)[223]	⟨100⟩ fiber	(100)[001]
	(1-10)[111]	—	(100)[0-13]
	(1-10)[332]	—	(100)[1-10]
	(1-10)[221]	⟨lvw⟩ fiber	(334)[1-10]
	(1-10)[331]	—	(112)[1-10]
	(1-10)[110]	—	(113)[1-10]
⟨210⟩ fiber	(210)[001]	—	(114)[1-10]
	(210)[−125]	—	(116)[1-10]
	(210)[−123]	—	—
	(210)[−122]	—	—
	(210)[−121]	—	—
	(210)[−120]	—	—

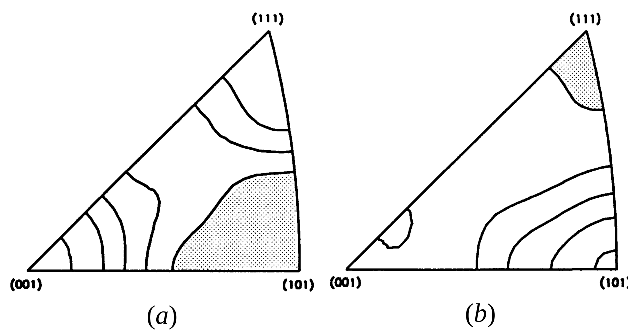

Fig. 10—Transformation textures predicted solely *via* selection of the positive slip variants for the (*a*) compression and (*b*) extension experiments.

⟨111⟩ and ⟨100⟩ fibers (Figure 9b, Table VI); to these were added five minor components that extend along the ⟨*1vw*⟩ fiber. These orientations were selected after careful examination of the measured deformation textures. In both the compression and extension predictions, the parents were weighted according to their corresponding relative intensities in the measured deformation textures.

For both sets of parent orientations, the slip activities and 24 possible K–S transformation variants were determined. The transformation components selected using the slip activity criterion for the compression and extension experiments are illustrated in Figures 10(a) and (b), respectively. These figures should be compared with Figures 8(a) and (b). In each case, the simulated textures deviate to some extent from the measured textures. In particular, the ⟨112⟩ component is absent from the pole figure that represents the positive slip variants of the compression experiment and the relative intensity of the ⟨001⟩ component is much too high. Similar criticisms apply to the reaction product variants shown in Figures 11(a) and (b). The reaction product variants for the compression experiment (Figure 11(a)) reproduce the experimental texture faithfully in the vicinity of the ⟨111⟩ and ⟨112⟩ fibers, while the minor ⟨100⟩ fiber is very weak. For the reaction products of the extension experiment, a texture intensity is visible near the ⟨532⟩ and ⟨210⟩ fibers (Figure 11(b)), which is not apparent in the experimental texture.

After combination of the two sets of variants for each

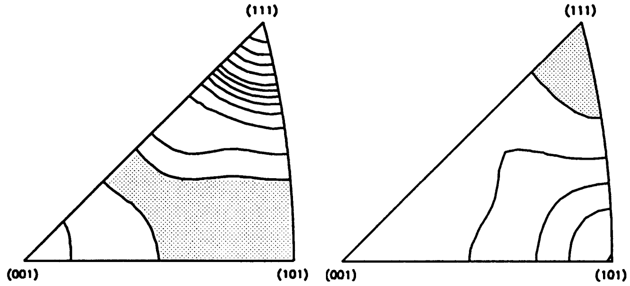

(*a*) (*b*)

Fig. 11—Transformation textures predicted solely *via* selection of the reaction product variants for the (*a*) compression and (*b*) extension experiments.

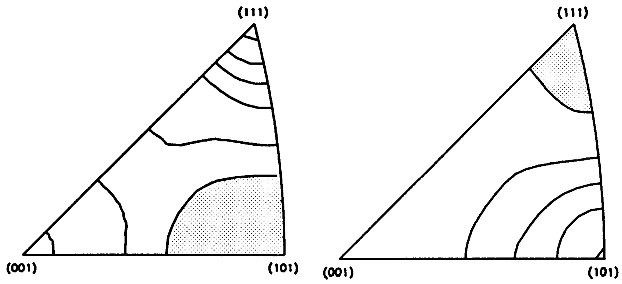

(*a*) (*b*)

Fig. 12—Transformation textures predicted using the present model for the (*a*) compression and (*b*) extension experiments. Here, the positive slip and reaction product variants have been combined in the ratio 1:1.5 and a random texture of approximately 35 pct was added.

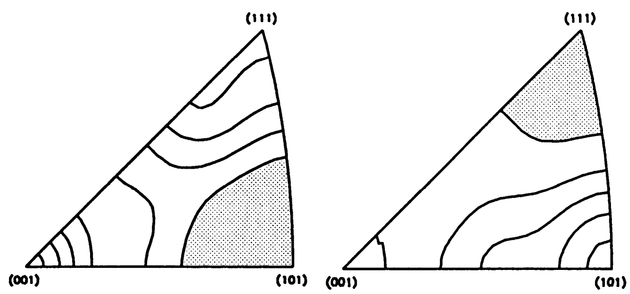

(*a*) (*b*)

Fig. 13—Transformation textures predicted solely *via* selection of the negative and no-reaction variants for the (*a*) compression and (*b*) extension experiments.

experiment in accordance with the dislocation reaction model, the overall predicted transformation textures are in excellent agreement with the actual transformation textures. As in the plane strain rolling case, the reaction product variants were given 1.5 times the weight of the positive slip variants. Figure 12(a) should be compared to Figure 8(a) (compression), and Figure 12(b) should be compared to Figure 8(b) (extension). In both cases, all the principal components are accounted for in the simulations. Again, it is clear that the positive slip and reaction product variants are *both* required if the experimental textures are to be accurately reproduced.

The inverse pole figures associated with the *rejected* variants are illustrated in Figures 13(a) and (b) for the compression and extension cases, respectively. Here, it can be seen that the rejected compression variants, if included, would lead to too high an intensity in the vicinity of ⟨001⟩. Similarly, in the extension case, inclusion of the rejected variants would introduce a minor component centered about ⟨210⟩, which is not observed.

VI. SIMPLE SHEAR

Application of the dislocation reaction model to deformation by simple shear proved to be far more difficult than to the previous strain paths, because complications were introduced by the lower symmetry of shear textures. An outline of the results and conclusions is provided in this section; a more complete description is provided elsewhere.[15]

A. *Experimental Approach*

To generate the experimental textures, a torsion sample (diameter = 8.8 mm) was machined from the Fe-30 pct Ni alloy and subjected to a von Mises strain of 3 at a strain rate of 0.1 s^{-1}. The servo-hydraulic torsion machine rotated in a counterclockwise direction, producing negative shear in the specimen. The ends of the specimen were not fixed, so that some lengthening occurred during testing. A heating rate of 1 °C/s was used to bring the specimen to the final testing temperature of 320 °C, at which it was held for 3 minutes prior to straining; this was followed by air cooling. The specimen was then sliced into two equal sections and one half was quenched in liquid nitrogen to induce the transformation to martensite.

Specimen preparation for texture measurements was an intricate process due to the absence of strain in the center of the sample (which was removed) and its centrosymmetric properties. For the sake of brevity, this process will not be described here. The neutron diffraction facilities at the Chalk River Laboratories of AECL were again used to measure the texture. Orientation distribution functions were calculated on the basis of cubic crystal and monoclinic sample symmetry from three complete pole figures for both the deformed and quenched specimens.

B. *Experimental Textures*

During deformation by torsion, a monoclinic texture develops in the specimen. This means that a Euler space of $\varphi_1 = 0$ to 180 deg, $\Phi = 0$ to 90 deg, and $\varphi_2 = 0$ to 90 deg is necessary to represent the texture completely. The ODF for the deformed torsion sample is illustrated in Figure 14(a). The texture is mainly comprised of the characteristic components of fcc shear, namely, A (1-11)[110], A_1* (−11-1)[−2-11], A_2* (1-11)[121], B (1-12)[110], and C (001)[110]. A continuous band of orientations extends in the φ_2 direction along the {111} fiber from A_1* through A to A_2*. The ⟨110⟩ fiber is also present and appears in two places: first, in the $\varphi_2 = 45$ deg section extending in the ϕ direction from orientation A through B to C and second in the φ_2 direction from C through B to A_2*/A_1*.

After quenching, the resulting textures are no longer strictly monoclinic; however, to avoid confusion, both the experimental and predicted transformation textures are displayed using ODFs applicable to monoclinic sample symmetry. (A detailed description of the triclinic texture is given

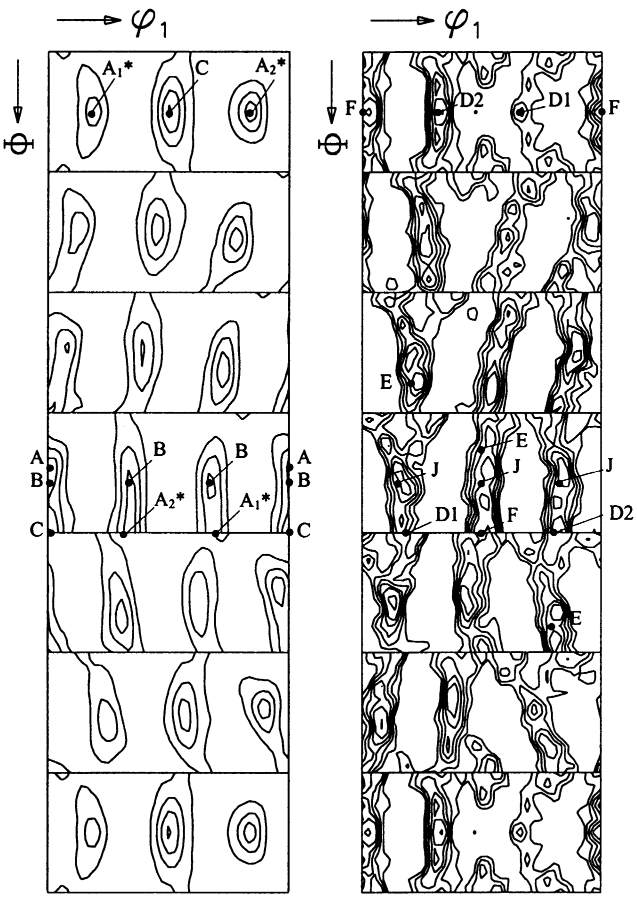

(*a*) (*b*)

Fig. 14—Measured (*a*) deformation and (*b*) transformation textures for the torsion sample.

in Reference 15.) An ODF of the measured transformation texture is shown in Figure 14(b). Quenching resulted in a significant change in the overall texture and the major orientations now visible are D1 (11-2)[111], D2 (−1-12)[111], E (01-1)[111], F (110)[001], and J (0-11)[−211]. Once again, there are continuous bands of orientations (*i.e.*, fibers) extending in the φ_2 and θ directions. The orientations run in part along the ⟨111⟩ fiber from D1 through E to D2. In addition, the {110} fiber extends from F through J to E, first in the $\varphi_2 = 45$ deg section and second along the φ_2 direction. The similarity of the preceding *transformation* components to the ideal orientations produced by bcc *shear* is not entirely coincidental. It originates from the equivalencies inherent in the K–S relations and the slip planes and directions involved in fcc and bcc slip.

Examination of the experimental textures revealed an asymmetry or "tilt" of the texture components of approximately 5 deg about the φ_1 or radial direction (*r*). Tilts of this nature are characteristic of torsion textures and have been reported in both fcc and bcc polycrystals.[18–21] To account for this tilt in the present predictions, the selected parent orientations were rotated by +5 deg about the φ_1 direction.

C. *Prediction of the Transformation Texture*

A careful examination of the experimental textures resulted in the selection of five major parent orientations and nineteen minor parents (Table VII). The five major parents are the well-established ideal fcc shear components, namely, A (11-1)[1-10], A_1* (−11-1)[−2-11], A_2*(1-11)[121], B (1-12)[110], and C (001)[110].[18,19,20] The need for such a large number of minor components arose due to the limitations imposed by specimen preparation and, in particular, the curvatures present in each small section (approximately 2 × 3 × 10 mm) of the sample. To predict the transformation texture, a procedure similar to that employed for the previous strain paths was applied to each of the 24 parents. This produced four sets of variants: positive slip, negative slip, reaction product, and miscellaneous. In some cases, the ideal starting orientations had to be rotated slightly away from ideal so as to activate more than one slip system in the crystal. The transformation variants were again weighted according to their shear values and their corresponding parent intensities. The estimated parent intensities for all the parents are listed in Table VII.

Figure 15(a) depicts the texture predicted solely *via* selection of the positive shear variants and should be compared to the experimental transformation texture shown in Figure 14(b). The orientations present in Figure 15(a) are situated near D1, D2, and E, while no components are visible in the vicinity of the F and J major orientations. The situation is reversed in Figure 15(b), in which only the reaction product variants are illustrated. In this ODF, the only major orientations predicted are close to F and J. In each case, the prediction varies notably from the measured transformation texture.

Once again, after integrating the positive slip and reaction product variants in a single ODF, the modeled texture provides an accurate reproduction of the measured transformation texture (Figure 15(c)). All the major peaks of the experimental texture, including their relative intensities, are accurately reproduced in the simulated texture. More specifically, the intensity of D1 is approximately half that of D2 in both the experimental and predicted ODFs.

The validity of the dislocation reaction model is further strengthened by examination of the transformation texture formulated *via* selection of the negative slip variants only (Figure 16(a). In this prediction, it is D1 rather than D2 that is the stronger component, and therefore, the experimental texture is not correctly reproduced. Furthermore, there are additional components, for example, ($\varphi_1 = 115$ deg, $\Phi = 40$ deg, and $\varphi_2 = 15$ deg) and ($\varphi_1 = 105$ deg, $\Phi = 35$ deg, and $\varphi_2 = 30$ deg), present in Figure 16(a) that are not observed in the measured texture. A similar situation rises in Figure 16(b), in which all the remaining variants are plotted, *i.e.*, those grouped as miscellaneous. In this instance, the cube {100}⟨001⟩ orientation appears as the major component of the predicted texture, whereas it is a very weak component in the experimental texture. From these results, it is clear that the dislocation reaction model provides an accurate representation of the transformation textures appearing after deformation by simple shear.

VII. IMPLICATIONS OF THE DISLOCATION GLIDE MODEL ON NUCLEATION AND GROWTH

It is well known that the γ-to-α' transformation involves three distinct physical components: (1) a lattice *expansion* (often associated with the Bain strain), (2) a lattice shear

Table VII.   Parent Orientations and Weights Used in the Torsion Simulations

Parent	Name	Miller Indices (No Tilt)	Euler Angles (No Tilt)	Parent Intensity
1	—	(001)[130]	180 90 108	0.2
2	—	(001)[120]	180 90 117	0.4
3	—	(001)[230]	180 90 124	0.6
4	C	(001)[110]	180 90 135	0.6
5	—	(1-15)[110]	180 106 135	1.0
6	—	(1-14)[110]	180 110 135	1.0
7	—	(1-13)[110]	180 115 135	1.0
8	B	(1-12)[110]	180 126 135	1.0
9	—	(2-30)[110]	180 133 135	1.0
10	A	(1-11)[110]	180 145 135	2.0
11	—	(1-11)[154]	165 143 117	0.6
12	—	(1-11)[132]	155 141 104	0.4
13	A_2*	(1-11)[121]	145 135 90	0.1
14	a_1*	(−11-1)[−2-11]	35 135 180	0.1
15	—	(−11-1)[−3-21]	25 141 165	0.5
16	—	(−11-1)[−5-41]	15 143 153	0.7
17	—	(1-12)[131]	160 120 98	0.8
18	—	(1-14)[6 10 1]	175 109 119	0.8
19	—	(1-12)[241]	165 122 108	0.8
20	—	(100 −30 −18)[−24 −100 32]	60 20 45	0.8
21	—	(100 −33 −27)[−20 −100 49]	60 30 45	0.8
22	—	(16 −100 34)[−100 −2 41]	125 30 45	0.8
23	—	(97 100 −58)[100 −73 42]	35 30 0	1.5
24	—	(67 −100 58)[−100 −50 29]	145 30 0	0.5

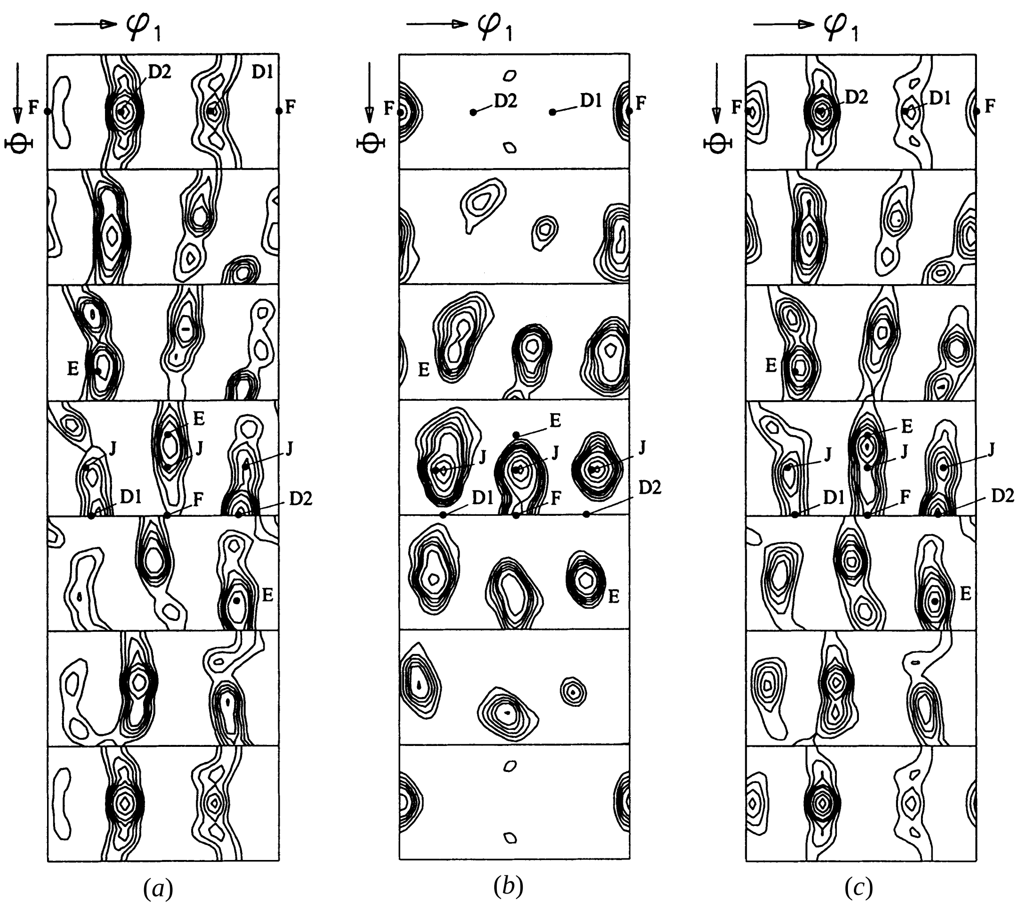

Fig. 15—Transformation textures predicted solely *via* selection of the (*a*) positive slip and (*b*) reaction product variants for the torsion experiment. (*c*) Transformation texture predicted using the present model for the torsion experiment. Here, the positive slip and reaction product variants have been combined in the ratio 1:1.5.

Table VIII. Pairs of {111}⟨110⟩ Cross-Slip-Related Slip Systems Capable of Producing {225} and {110} Shears

Bishop and Hill Nomenclature	Active Slip Systems	Resultant Shears {225} Type	Resultant Shears {110} Type
$a_I + c_I$	$(111)\langle 01\bar{1}\rangle + (\bar{1}11)\langle 01\bar{1}\rangle$	$(522)\langle 01\bar{1}\rangle$ and $(5\bar{2}\bar{2})\langle 01\bar{1}\rangle$	$(011)\langle 01\bar{1}\rangle$
$b_I + d_I$	$(\bar{1}\bar{1}1)\langle 0\bar{1}\bar{1}\rangle + (1\bar{1}1)\langle 0\bar{1}\bar{1}\rangle$	$(52\bar{2})\langle 0\bar{1}\bar{1}\rangle$ and $(5\bar{2}2)\langle 0\bar{1}\bar{1}\rangle$	$(0\bar{1}1)\langle 0\bar{1}\bar{1}\rangle$
$b_{II} + c_{II}$	$(\bar{1}\bar{1}1)\langle 101\rangle + (\bar{1}11)\langle 101\rangle$	$(\bar{2}52)\langle 101\rangle$ and $(25\bar{2})\langle 101\rangle$	$(\bar{1}01)\langle 101\rangle$
$a_{II} + d_{II}$	$(111)\langle \bar{1}01\rangle + (1\bar{1}1)\langle \bar{1}01\rangle$	$(252)\langle \bar{1}01\rangle$ and $(\bar{2}5\bar{2})\langle \bar{1}01\rangle$	$(101)\langle \bar{1}01\rangle$
$a_{III} + b_{III}$	$(111)\langle 1\bar{1}0\rangle + (\bar{1}\bar{1}1)\langle 1\bar{1}0\rangle$	$(225)\langle 1\bar{1}0\rangle$ and $(\bar{2}\bar{2}5)\langle 1\bar{1}0\rangle$	$(110)\langle 1\bar{1}0\rangle$
$c_{III} + d_{III}$	$(\bar{1}11)\langle \bar{1}\bar{1}0\rangle + (1\bar{1}1)\langle \bar{1}\bar{1}0\rangle$	$(\bar{2}25)\langle \bar{1}\bar{1}0\rangle$ and $(2\bar{2}5)\langle \bar{1}\bar{1}0\rangle$	$(\bar{1}10)\langle \bar{1}\bar{1}0\rangle$

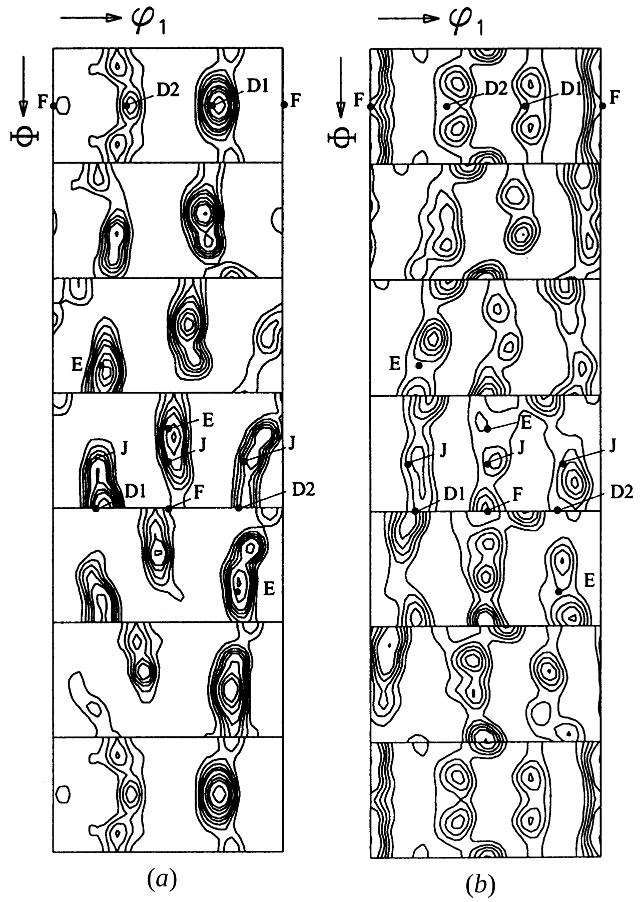

Fig. 16—Transformation texture predicted solely *via* selection of the (*a*) negative slip and (*b*) miscellaneous and no-reaction variants for the torsion experiment.

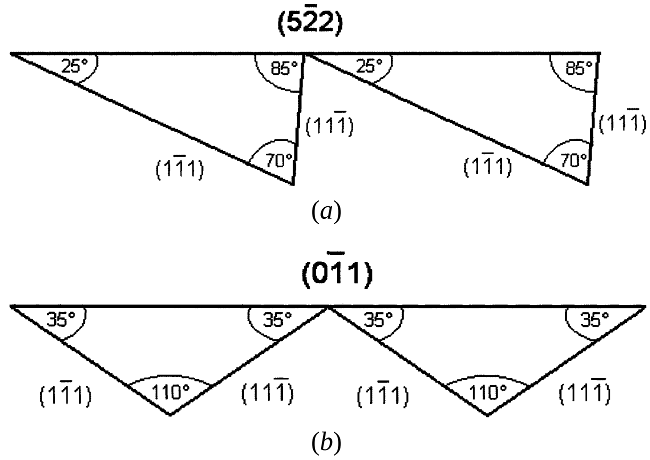

Fig. 17—Illustration of how glide along a pair of cross-slip-related slip systems can produce a resultant [011] type shear along the (*a*) (5$\bar{2}$2) and (*b*) (0$\bar{1}$1) planes.

(either by slip or by twinning), and (3) a rigid body *rotation*.[22] It is therefore intriguing to consider what the present results indicate regarding the particular step that controls variant selection. As the stresses associated with the Bain strain have been linked with the *nucleation* step, the lack of relative importance of this strain seems to suggest that only minor amounts of variant selection occur at the nucleation stage. In a similar manner, setting both twinning and the rigid body rotation aside for the moment as being of secondary importance, attention will be focused on the evident role of dislocation glide and, therefore by inference, of the *growth* process.

During the formation of martensite and bainite, lattice shear is expected to take place at the γ/α' interface, which is also known as the habit plane. Because the latter is $\{111\}_\gamma$ in low and medium plain C steels and, furthermore, because all the transformation theories call for the Burgers vectors to be of the $\langle 110\rangle_\gamma$ type,[22] it is clear that the $\{111\}\langle 110\rangle_\gamma$ dislocations that play such an important role in the present model can be considered to favor the growth of certain variants over others. Less clear is how the {111}⟨110⟩ dislocations discussed here participate in other materials, where habit planes such as the {225}, {557}, or {112} are observed.[23] Transformation theory also calls for the lattice shear to be of the $\{110\}\langle 110\rangle_\gamma$ type under certain conditions.[22]

It is of interest that such resultant shears could consist of sums of cross-slip-related {111}⟨110⟩ type shears. A schematic diagram showing how the combined occurrence of $(1\bar{1}1)[0\bar{1}\bar{1}]$ and $(\bar{1}11)[0\bar{1}\bar{1}]$ glide can lead to resultant shears of $(5\bar{2}2)[0\bar{1}\bar{1}]$ and $(0\bar{1}1)[0\bar{1}\bar{1}]$ is presented in Figure 17. The full list of possible cross-slip-related slip systems for the two types of resultant planes is given in Table VIII. Here, it can be seen that all the possible combinations of {111}⟨110⟩ systems provide totals of 12 {225} and 6 {110} shear planes. Similar diagrams (with different angles) can be prepared for any {*hhl*} habit plane.

Returning to the seven deformed parent crystals of Table IV, it is clear that they all contain cross-slip-related shears, which, when summed, can produce the resultant {225}⟨110⟩, {557}⟨110⟩, {112}⟨110⟩, or {110}⟨110⟩ shear observed by numerous workers or called for by the various transformation theories. Similar remarks apply to the grains deformed along the other three strain paths. These observations thus support the unexpected requirement of the present model for cross-slip to occur after the formation of certain reaction products. This additional operation is then able to provide the cross-slip components required for propagation of the transformation that have not already been produced directly by the glide process.

Although a good case can be made that the presence of glide, reaction, and cross-slip dislocations favors the growth of certain variants, as discussed previously, clearly, considerable further work is required to determine whether the dislocations called for in the preceding analysis are actually present at the γ/α' interface and play the roles proposed here.

VIII. CONCLUSIONS

The dislocation reaction model for variant selection during the γ-to-α' transformation[1] was originally derived by analyzing the experimental results of Liu and Bunge.[9] The two selection criteria specify that only those K–S variants associated with active slip systems and with their permissible in-plane dislocation reaction products are selected. In this investigation, samples of Fe-30 pct Ni were deformed along four distinct strain paths (plane strain rolling, axisymmetric compression, axisymmetric extension, and simple shear) and then transformed by quenching in liquid nitrogen. Both the deformation and transformation textures were measured. The model was then applied to the main components of the deformation textures, leading to the predicted or simulated textures described earlier. For the four strain paths studied, the following conclusions can be drawn.

1. Prediction of the transformation texture solely *via* selection of the positive slip variants produces a texture that varies substantially from the measured transformation texture. Similar remarks apply to the predictions based solely on the reaction product variants.
2. When the positive slip and reaction product variants are combined according to the present model, the ensuing textures are in excellent agreement with the experimental findings.
3. Selection of the negative slip, no-reaction, and miscellaneous variants yields product orientations that are not present in the respective measured transformation textures. Consequently, the overall textures predicted without the use of variant selection differ significantly from the measurements.
4. The dislocation reaction model is capable of reproducing the transformation textures produced after deformation by plane strain rolling, axisymmetric compression and extension, and simple shear, and therefore, it appears to be of wide validity.
5. An interesting feature of the present theory is that pairs of cross-slip-related $\{111\}\langle 110\rangle$ type glide events can provide resultant shears of the $\{110\}\langle 110\rangle$, $\{111\}\langle 110\rangle$, $\{112\}\langle 110\rangle$, $\{557\}\langle 110\rangle$, and $\{225\}\langle 110\rangle$ type called for by experimental observations as well as by some of the transformation theories. The lattice shears provided by movement of these dislocations along the γ/α' interface suggest that growth (as opposed to nucleation) controls variant selection during transformation.

ACKNOWLEDGMENTS

The authors express their gratitude to the Natural Sciences and Engineering Research Council of Canada for the financial support of this investigation and to Professor Druce Dunne, University of Wollongong, for providing the experimental material. In addition, the authors thank Mr. Joseph Azar for permission to use his slip activity program and Mr. Patrick Wilson, AECL, for producing the axisymmetric extension specimens.

REFERENCES

1. M. Sum and J.J. Jonas: *Textures Microstr.*, 1999, vol. 31, pp. 187-215.
2. M.P. Butrón-Guillén, C.S. da Costa Viana, and J.J. Jonas: *Metall. Mater. Trans., A*, 1997, vol. 28A, pp. 1755-68.
3. J.C. Bokros and E.R. Parker: *Acta Metall.*, 1963, vol. 11, pp. 1291-1301.
4. M. Humbert, F. Wagner, W.P. Liu, C. Esling, and H.J. Bunge: *Proc. 8th Int. Conf. on Textures of Materials (ICOTOM 8)*,, TMS-AIME, Warrendale, PA, 1988, pp. 743-54.
5. J.R. Patel and M. Cohen: *Acta Metall.*, 1953, vol. 1, pp. 531-38.
6. J.F. Bishop and R. Hill: *Phil. Mag.*, 1951, vol. 42, pp. 414-27.
7. J.F. Bishop and R. Hill: *Phil. Mag.*, 1951, vol. 42, pp. 1298-1307.
8. G. von Kurdjumov and G. Sachs: *Z. Phys.*, 1930, vol. 64, pp. 325-43.
9. W.P. Liu and H.J. Bunge: *Mater. Lett.*, 1991, vol. 10. pp. 336-43.
10. J.J. Jonas and N.J. Wittridge: *Proc. 12th Int. Conf. on Textures of Materials (ICOTOM 12)*, Montreal, Aug. 1999, National Research Council of Canada, Chalk River, pp. 1049-58.
11. J.J. Jonas and N.J. Wittridge: *Met. Mater. (Korea)*, 2000, vol. 6, pp. 211-20.
12. J.J. Jonas and N.J. Wittridge: *Proc. of the NATO Advanced Study Institute of Multiscale Phenomena in Plasticity*, J. Lépinoux, D. Mazière, V. Pontikis, and G. Saada, eds., Kluwer Academic Publishers B.V., Dordrecht, 2000, pp. 143-56.
13. N.J. Wittridge, J.J. Jonas, and J.H. Root: *Proc. 12th Int. Conf. on Textures of Materials (ICOTOM 12)*, Montreal, Aug. 1999, National Research Council of Canada, Ottawa, pp. 1089-94.
14. M. Sum, J.J. Jonas, and J.H. Root: *Proc. 12th Int. Conf. on Textures of Materials (ICOTOM 12)*, Montreal, Aug. 1999, National Research Council of Canada, Ottawa, pp. 761-66.
15. N.J. Wittridge and J.J. Jonas: *Acta Mater.* 2000, vol. 48, pp. 2737-49.
16. J. Weertman and J.R. Weertman: *Elementary Dislocation Theory*, Oxford University Press Inc., New York, NY, 1992.
17. L. Kaufman and M. Cohen: *Trans. AIME, J. Met.*, 1956, pp. 1393-1401.
18. L.S. Tóth, K.N. Neale, and J.J. Jonas: *Int. J. Plasticity*, 1989, vol. 6, pp. 45-52.
19. L.S. Tóth, J.J. Jonas, P. Gilormini, and B. Bacroix: *Int. J. Plasticity*, 1990, 6, pp. 83-108.
20. F. Montheillet, M. Cohen, and J.J. Jonas: *Acta Metall.*, 1984, vol. 32 (11), pp. 2077-89.
21. J. Baczynski and J.J. Jonas: *Acta Mater.*, 1996, vol. 44 (11), pp. 4273-88.
22. D.A. Porter and K.E. Easterling: *Phase Transformations in Metals and Alloys*, Chapman and Hall, London, 1981.
23. P.G. McDougall and C.M. Wayman: in *Martensite: A Tribute to Morris Cohen*; G.B. Olson and W.S. Owen, eds., ASM INTERNATIONAL, Materials Park, OH, pp. 59-95, 1992.